Mechanical tuning of a rectangular axion haloscope operating around 8.4 GHz

Jessica Golm [1,2,*]**, Jose María García-Barceló** [3,*]**, Sergio Calatroni** [1]**, Walter Wuensch** [1]**, Babette Döbrich** [3]

[1] *CERN - European Organization for Nuclear Research, Geneva, Switzerland*
[2] *Friedrich Schiller University Jena (Institute for Optics and Quantum Electronics), Jena, Germany*
[3] *Max-Planck-Institut für Physik (Werner-Heisenberg-Institut), Boltzmannstr. 8, 85748 Garching bei München, Germany*

Correspondence*:
Jessica Golm, Jose María García-Barceló
jessica.golm@cern.ch, jmgarcia@mpp.mpg.de

ABSTRACT

The axion haloscope is the currently most sensitive method to probe the vanishingly small coupling of this prominent Dark Matter candidate to photons. To scan a sizeable axion Dark Matter parameter space, the cavities that make up the haloscope need to be tuned efficiently. In this article, we describe a novel technique to tune axion haloscopes around 8.4 GHz in a purely mechanical manner without the use of dielectrics. We achieve tuning by introducing a gap along the cavity geometry. Losses are added due to the leaking of the field out of the structure only if the gap becomes too large concerning the total width. A tuning range of around 600 MHz is achieved, depending on the environmental conditions. We present the results of a corresponding prototype and outline prospects to further develop this technique.

1 INTRODUCTION

An axion haloscope is an experimental apparatus used in the search for axions, hypothetical particles that could make up Dark Matter in the Universe as discussed in Peccei and Quinn (1977b,a). In recent years, there has been a large increase in the number of experiments and approaches that aim to find or exclude the axion as Dark Matter, see e.g. here Irastorza and Redondo (2018).

Axions are very light, neutral particles that are expected to interact very weakly with ordinary matter and electromagnetic fields. Axion haloscopes are designed to detect axions by converting them into detectable electromagnetic signals (photons) in the presence of a strong magnetic field by the inverse Primakoff effect, cf. Primakoff (1951). To improve this conversion process, haloscopes use high-quality factor resonators, such as microwave cavities, see e.g. here Sikivie (1983). The conversion of axions into photons occurs when the mass of the axion matches approximately the resonant frequency of the apparatus.

The primary goals of an effective axion detection system involve maximising the power generated from the axion-photon interaction and expanding the range of analysed axion masses (i.e. the range of frequencies scanned). The detected radio frequency (RF) power (P_d) relies on inherent axion properties and experimental cavity characteristics, as outlined in Díaz-Morcillo et al. (2022):

$$P_d = \kappa \, g_{a\gamma}^2 \, \frac{\rho_a}{m_a} \, B_e^2 \, C \, V \, Q_l, \tag{1}$$

Here, κ signifies the coupling to the external receiver ($\kappa = 0.5$ for critical coupling operation), $g_{a\gamma}$ represents the unknown axion-photon coupling, ρ_a denotes Dark Matter density, m_a stands for axion mass, B_e represents the external static magnetic field (dependent on the magnet used in the experiment), C is a label for the so-called 'form factor', V is the cavity volume, and Q_l represents the loaded quality factor of the cavity. In contrast to Q_l, the unloaded quality factor Q_0 is a common metric in characterising resonant cavities as it is independent of external coupling, see e.g. here Pozar (2012); Rezaee et al. (2012). The form factor (C), measuring the coupling between the external magnetostatic field and the RF electric field induced by axion-photon conversion, is expressed as:

$$C = \frac{|\int_V \vec{E} \cdot \vec{B}_e \, dV|^2}{\int_V |\vec{B}_e|^2 \, dV \int_V \varepsilon_r \, |\vec{E}|^2 \, dV}, \tag{2}$$

Here, ε_r represents the relative electrical permittivity within the cavity of volume V. The sensitivity measure of the haloscope is the axion-photon coupling detectable for a given signal-to-noise ratio ($\frac{S}{N}$), which can be calculated using:

$$g_{a\gamma} = \left(\frac{\frac{S}{N} \, k_B \, T_{sys}}{\kappa \, \rho_a \, C \, V \, Q_l} \right)^{\frac{1}{2}} \frac{1}{B_e} \left(\frac{m_a^3}{Q_a \, \Delta t} \right)^{\frac{1}{4}}, \tag{3}$$

In this equation, k_B represents the Boltzmann constant, T_{sys} is the noise temperature of the system, Q_a represents the quality factor of the axion resonance, and Δt is the data-taking time window, cf. Díaz-Morcillo et al. (2022). To summarise, the controllable parameters in a given experimental set-up encompass κ, C, V, and Q_l.

On the other hand, the mass of axions, if they exist, is not known. To maximise the chances of detecting axions, the haloscope needs to be tuned to the resonant frequency that corresponds to the expected mass range of axions being searched for. Tuning ensures that the cavity is effectively only sensitive to the specific axion masses under investigation, improving the chances of successful detection. Thus, the scanning rate $\frac{dm_a}{dt}$ is commonly employed to assess the performance of a haloscope, a value derived from Equation 3, cf. Kim et al. (2020):

$$\frac{dm_a}{dt} = Q_a \, Q_l \, \kappa^2 \, g_{a\gamma}^4 \left(\frac{\rho_a}{m_a} \right)^2 B_e^4 \, C^2 \, V^2 \left(\frac{S}{N} \, k_B \, T_{sys} \right)^{-2}. \tag{4}$$

Also, κ is usually rewritten in terms of the coupling coefficient β, which can be extracted from the expression

$$\beta = \frac{\kappa}{1 - \kappa}. \tag{5}$$

A tuning step must not require the opening of the cryostat as this is very time and energy-consuming. Until today, most of the adjustment techniques applied in haloscope experiments for frequency tuning have relied on mechanical systems. Various collaborations such as ADMX (cf. Boutan et al. (2018)), HAYSTAC (cf. Zhong et al. (2018)), and IBS/CAPP (cf. Choi et al. (2021)) utilise cylindrical cavities

with metallic rods. These rods are rotated inside the cavities, altering the electromagnetic field distribution and, consequently, the resonant frequency of the operating mode. This rotation is achieved either through several gears connected to a motor or by employing piezoelectric elements. A slightly different technique was, for example, employed by the QUAX collaboration (cf. Alesini et al. (2020)), by using adjustable sapphire shells to modify the resonant frequency of the cavity. In a different example, the CAST-CAPP/IBS group uses two movable dielectric sapphire plates positioned symmetrically at the cavity sides (see e.g. here Miceli (2015)). In Kuo (2021) tunable conic shell-cavities have been investigated, providing good tuning results for large cavities operating around 7.5 and 20 GHz. Table 1 gives an examination of some current tuning systems for frequencies between 4 and 11 GHz, in comparison with the outcomes obtained in this work. The percentage value of tuning has been calculated according to the following equation

Experiment	Freq. (GHz)	Tuning (%)	$Q_0/10^4$	C	References
CAST-CAPP	$4.774 - 5.174$	7.7	~ 4	~ 0.53	Adair et al. (2022)
ADMX Sidecar - Run B	$5.086 - 5.799$	12.3	$0.22 \times (1 + \beta)$	$0.44 - 0.61$	Boutan et al. (2018)
HAYSTAC	$5.6 - 5.8$	3.45	1.8	~ 0.5	Zhong et al. (2018)
ADMX Sidecar - Run C	$7.173 - 7.203$	0.42	$0.23 \times (1 + \beta)$	$0.040 - 0.046$	Boutan et al. (2018)
RADES - Vertical Cut	$7.753 - 8.420$	9.52	$1.5 - 2.7$	~ 0.66	this work
QUAX	$10.1 - 10.3$	2	~ 9	$\sim 0.11/V$	Braggio et al. (2023)

Table 1. Overview of some existing tunable haloscopes operating at frequencies between 4 and 11 GHz. For the last row, the form factor is given in terms of volume (C/V), where V is in L. Also, for the second and fourth rows, the unloaded quality factor parameter has been left dependent on the β coupling employed for each corresponding experiment.

$$\text{Tuning} = \frac{f_2 - f_1}{f_2} \times 100 \quad [\%], \tag{6}$$

where f_2 is the upper limit in the frequency tuning range and f_1 is the lowest frequency. It is worth mentioning that the ADMX Sidecar experiment has conducted axion data taking campaigns using two different resonance modes. For Run B, this group has employed the TM_{010} mode, while for Run C they have used TM_{020}, to explore higher frequencies, where significantly lower form factor values are achieved. On the other hand, the CADEx collaboration proposed in Aja et al. (2022) the use of a sliding or tunable wall mechanism in rectangular cavities. The ORGAN group, in McAllister et al. (2023), also describes this type of mechanical tuning in detail, comparing it with the tuning technique using metal rods usually employed in the axion community. In addition, the QUAX group has explored in Braggio et al. (2023) opening techniques in a cylindrical cavity using angular misalignment on the longitudinal axis, achieving satisfactory results at frequencies above 10 GHz, using a so-called 'clamshell' cavity.

It should be mentioned that there is also the possibility of broad-band search, which removes the need of tuning, but typically cannot achieve a signal amplification comparable to the resonant haloscopes. Examples of such experiments are BRASS (magnetic mirror), see Bajjali et al. (2023), MADMAX (with a set of movable dielectric disks in Brun et al. (2019)), ALPHA (using metamaterials), cf.Gelmini et al. (2020), or BREAD, see Knirck et al. (2023).

Over the past five years, the RADES (Relic Axion Dark-Matter Exploratory Setup) research group has extensively explored haloscopes, engaging in the conceptualisation, production, and physics analysis of axion detectors in the pursuit of detecting Dark Matter axions with masses approximately around 1 and $34 \, \mu\text{eV}$, cf. Álvarez Melcón et al. (2018, 2020, 2021); Díaz-Morcillo et al. (2022); Ahyoune et al. (2023). This team has developed a mechanical tuning technique where the haloscope volume is increased by

mechanically moving the cavity halves split symmetrically (cf. Arguedas-Cuendis et al. (2020)), operating at X-band frequencies. This set-up can work similarly to the clamshell technique (cf. Braggio et al. (2023)), but a symmetric opening is more favourable, giving a bigger frequency tuning range, as shown below. Also, the RADES group is currently exploring other methods based on electrical tuning by the use of ferroelectric materials (see e.g. here García Barceló et al. (2023)).

In this work, our goal is to build a tuning mechanism that can tune the resonant frequency of the first RADES cavity (cf. Álvarez Melcón et al. (2018)) at 4 K by using the tuning technique presented in Arguedas-Cuendis et al. (2020). This haloscope is based on an array of five subcavities interconnected by waveguide irises to increase the total volume while maintaining a high resonant frequency for operation in dipole magnets. The frequency tuning approach presented in this study relies on the separation of two symmetrical halves until RF leakage through the aperture becomes the primary factor affecting Q_0. In the case of small apertures in this haloscope, the effect of a vertical cut along the longitudinal direction is negligible, as the microwave currents of the fundamental mode TE_{101} are parallel to this plane. This movement effectively increases the width of the cavity, thereby altering the search range for axion frequencies. According to Arguedas-Cuendis et al. (2020), the theoretical tuning range value for this haloscope is around 10 %. Similar values are also obtained in García-Barceló et al. (2023) for this type of tuning at X-band frequencies in other cavities. For this study, experiments are carried out at cryogenic temperatures, and simulations using the finite element method are employed to comprehend how the cavity behaves at various openings.

2 CAVITY DESIGN FOR MECHANICAL TUNING

Fig. 1 shows the schematics of the mechanical tuning idea. By introducing a gap between two cavity halves the geometry can be widened which shifts the resonant frequency to lower frequencies[1].
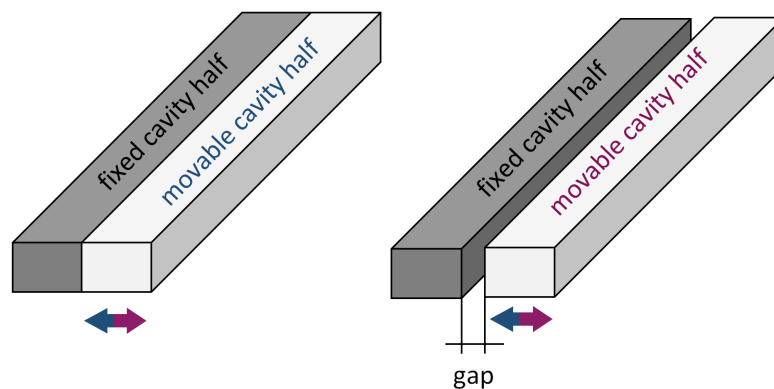

Figure 1. Schematics of the tuning concept. The left side shows the cavity in the closed position with no gap and at its highest resonant frequency. On the right side, a gap was introduced between the two cavity halves, tuning the cavity to a lower frequency depending on the gap size.

---

[1] In García-Barceló et al. (2023), preliminary investigations have been conducted with this technique for rectangular long single cavities, and 1D and 2D multicavity structures operating at X-band frequencies. A similar research is expected for the long single cavities, and 1D and 2D haloscopes with cylindrical shapes explored in García-Barceló et al. (2023).

2.1 Cavity design

The tuning mechanism will be exemplified using multi-cell cavities, which were developed by the RADES team, as described in Álvarez Melcón et al. (2018). This design allows an increase in cavity volume while maintaining a high resonant frequency as a single element of the cavity mostly determines the frequency. A prototype resonating at 8.4 GHz was built by joining five cells with all-inductive irises (vertical windows in waveguide technology). While the tuning will be demonstrated with this prototype, it works in principle for other designs as well.

Fig. 2 shows the electric field distribution of the five configuration modes. The coherence between the
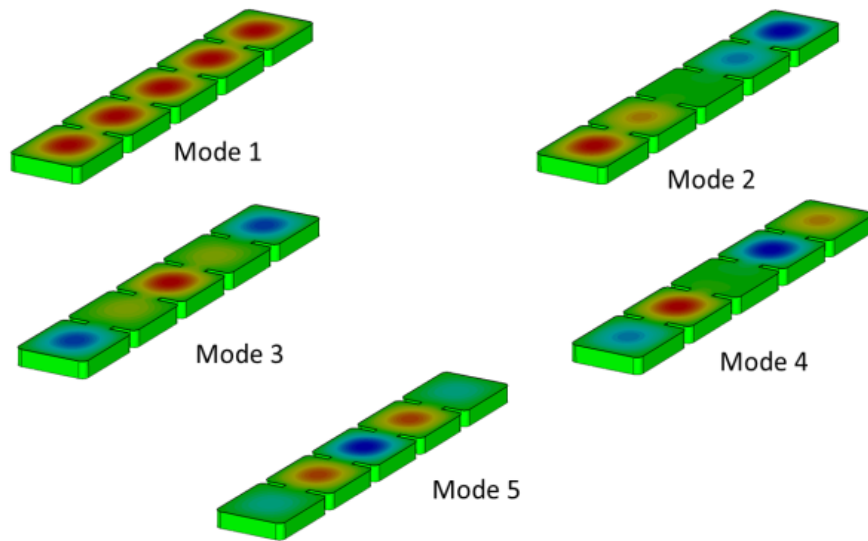
Figure 2. Electric field pattern for the five electromagnetic modes of the cavity. Red colour refers to a maximum and blue colour to a minimum in the electric field. Taken from Álvarez Melcón et al. (2018).

cavities is maintained only in the first mode which is the only mode that couples to the axion. To tune this type of cavity, it was cut along the symmetry plane as indicated in Fig. 3 (left). The surface currents do
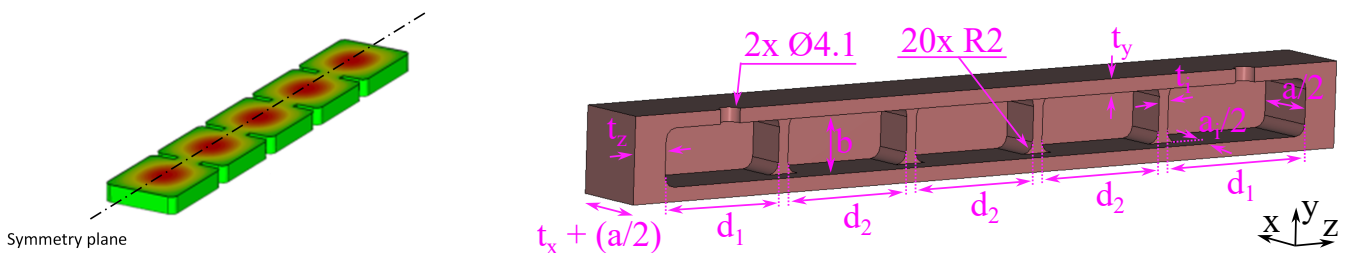

Figure 3. Left: Mode pattern with symmetry plane. The fabrication is done in two halves defined by this symmetry plane. 3D model housing of the vertical cut inductive irises cavity to be manufactured (right). This piece is one of the two symmetrical halves, which must be parallel. SMA coaxial ports are situated at the $\varnothing 4.1$ holes. Dimensions given in Table 2.

not cross this plane of symmetry (they are parallel to this plane); therefore, it is possible to cut the cavity without intercepting the current. Thus, one can expect to retain a high Q_0 value despite the introduction

of the manufacturing cut and even when separating both halves. This paper aims to study and measure to what extent this is possible.

To enable vertical cut tuning, small changes in the design of the 5-cell cavity (with manufacturing horizontal cut), described in Álvarez Melcón et al. (2018), were necessary. This cut can be used to introduce a gap that increases the volume and moves the resonant modes to lower frequencies, as shown in Fig. 1, without a significant loss of quality factor, as will be shown in the following. For this purpose, the gap should be small compared to the cavity dimensions ($< 10\,\%$ of the width, a value extracted from García-Barceló et al. (2023), where a similar tuning mechanism is employed). Fig. 3 (right)[2] depicts the 3D model and dimensions of the analysed haloscope. In Table 2, the dimension values are shown.

Dimensions	Values (in mm)
a	22.86
b	10.16
d_1	26.68
d_2	25
a_i	8
t_i	2
t_x	2.5
t_y	2.5
t_z	6.5

Table 2. Dimension values of the vertical cut haloscope for cryogenic conditions analysed in this study.

2.2 Simulations of losses introduced due to mechanical tuning

2.2.1 Parallel cavity halves

Before the manufacturing and measurements of this haloscope, a study was carried out using the Computer Simulation Technology (CST) Studio Suite software (2023), to study the behaviour of this structure in terms of Q_0 and C factors against different openings that can cause radiation losses.

Fig. 4 depicts the results obtained with a sweep of vertical cut gaps from 0 to 4 mm. For these simulations, an electrical conductivity value in the copper cavity of $\sigma_c = 10^9$ S/m was used, as this is a realistic value according to Golm et al. (2022) where the same coating and frequency were applied. In addition, coaxial antenna lengths have been chosen to be critically coupled ($\beta = 1$) for Port 1 and very undercoupled ($\beta \simeq 0$) for Port 2, in the closed scenario (gap$= 0$ mm). The antenna lengths have been maintained for the study of all the gap values.

As can be seen, the obtained form factor follows a relatively constant value, close to $C = 0.66$, for the whole range. However, the unloaded quality factor suffers a small detriment when the gap increases. For the full range of gaps analysed, the figure of merit $Q_0 V^2 C^2$ remains almost constant at around 11.5 L, so it can be guaranteed that the tuning range is adequate, obtaining a frequency tuning range of 1.07 GHz (or $12.6\,\%$), which is a very satisfactory tuning compared to the results of other experimental groups shown in Table 1, and even more so for operating frequencies close to 8.4 GHz.

---

[2] In the fabrication of these parts, alignment pins were included in the $x-$axis, in the thickness t_z of the housing at both ends in length. In addition, screw holes were implemented both in the port sections ($y-$axis) and in the t_z-thickness ($x-$axis). The latter to test the behaviour of the completely closed and screwed-together structure.
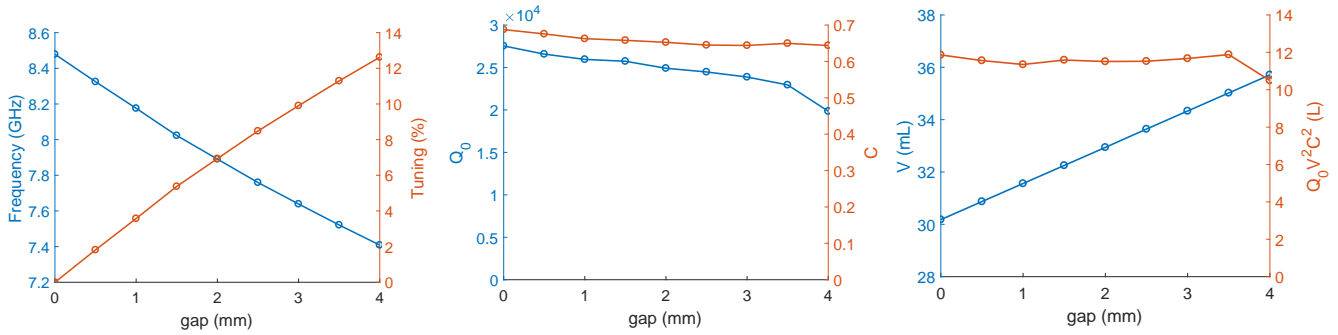
Figure 4. Results from CST simulations for the vertical cut tuning study applied in the haloscope depicted in Figure 3 (right): frequency and tuning versus gap (left), unloaded quality and form factors versus gap (centre), and volume and figure of merit ($Q_0 V^2 C^2$) versus gap (right).

In addition, since this structure has a tuning system that connects to the outside environment, a study has been made of possible signals that could enter its interior. After several simulations, it has been verified that there are no resonance echoes of a potential dipole magnet with a bore diameter of about 50 mm where this haloscope could be installed.

2.2.2 Misalignment studies

A simulation study has been conducted to consider possible misalignment effects when separating the two halves. Due to the position of the coaxial ports, the number of possible main misalignments is reduced to the following: angular $y-$axis, angular $z-$axis, and lineal $y-$axis. Fig. 5 shows an example of misalignment for each scenario. In addition, to reduce complexity, this tuning technique is based on leaving the coaxial
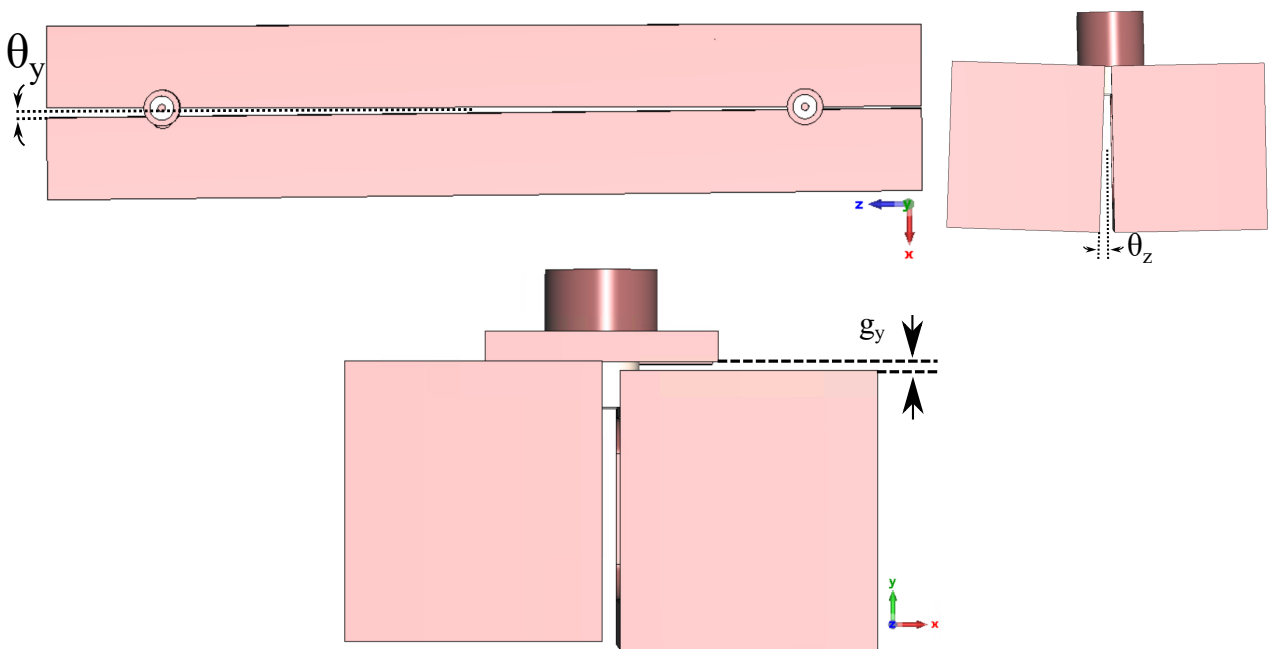

Figure 5. Misalignment effect in the vertical cut haloscope for three scenarios: angular $y-$axis (top left), angular $z-$axis (top right), and lineal $y-$axis (bottom).

ports attached to one of the halves of the haloscope. This introduces a small asymmetry between the two halves which can be neglected (see Appendix A).

Also, to simplify this investigation of misalignments, a gap of 1 mm has been chosen. Fig. 6 depicts the results obtained for each case as a function of the misalignment variables: θ_y for the angular $y-$axis, θ_z for the angular $z-$axis, and g_y for the linear $y-$axis. As can be seen, the results show a degradation in the
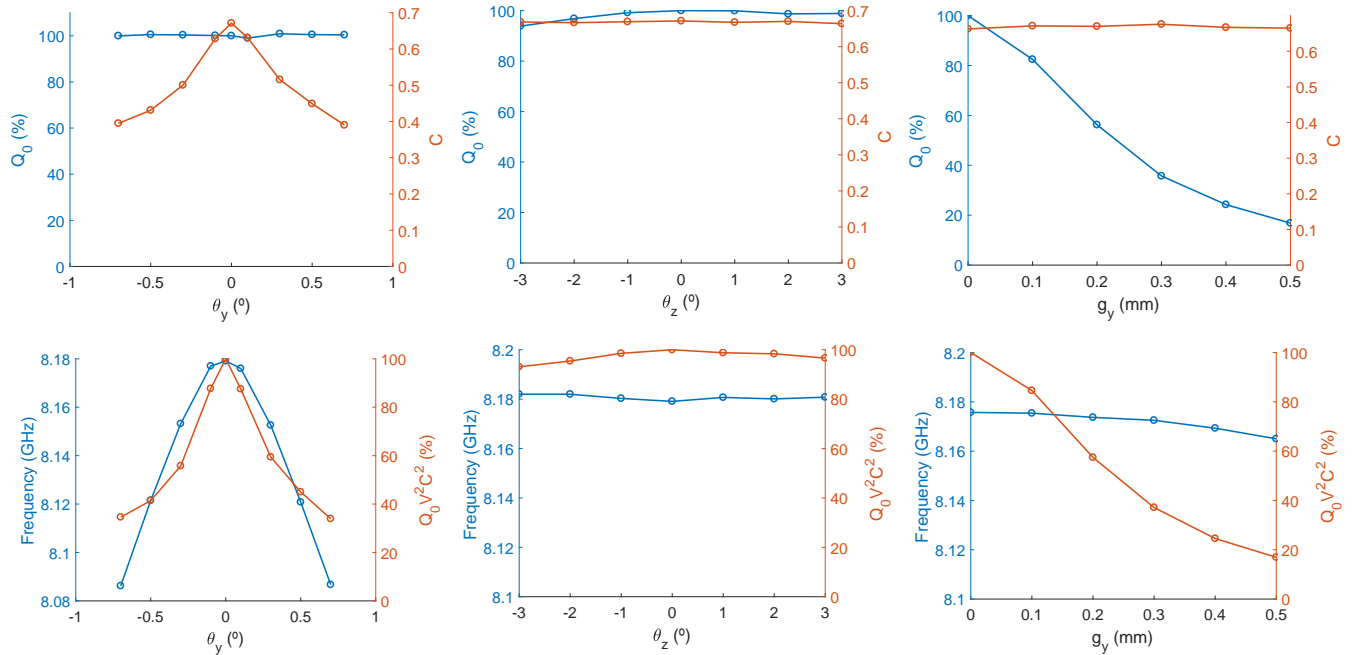
Figure 6. Results obtained in the simulation of the misalignment study in the angular $y-$axis (first column), in the angular $z-$axis (second column), and in the lineal $y-$axis (third column). The first row of graphs shows the variation of the quality and form factors versus the variation of the misalignment variable. The second row plots the variation in frequency and figure of merit $Q_0 V^2 C^2$ versus misalignment. The quality factor and figure of merit parameters are given in terms of the percentage change from the aligned scenarios ($\theta_y = \theta_z = g_y = 0$).

form factor value of $\sim 40\,\%$ in the case of angular misalignment in the $y-$axis. The main reason for this reduction is because the individual resonant frequencies of the subcavities are very sensitive to their widths, which are modified with θ_y, in turn changing the optimised condition for the operating mode (see more on this concept in Álvarez Melcón et al. (2018)). Furthermore, for this type of misalignment, the resonant frequency changes considerably (around $1.2\,\%$). However, the unloaded quality factor remains relatively stable.

On the other hand, for angular $z-$axis misalignment, the form factor remains very high, although the quality factor suffers a reduction of more than $7\,\%$ for negative values of θ_z. However, as the form factor becomes more important here for the figure of merit of the experiment, the latter remains relatively high. In the case of frequency, it is also maintained around stable values.

Finally, in the case of linear misalignment in the $y-$axis, it is seen that this causes the largest decrease of the unloaded quality factor (more than $80\,\%$ for values of $g_y = 0.5$ mm), while the form factor remains high for the entire range, and this in turn reduces the figure of merit the most of the three cases analysed. Fortunately, the outcomes show a resonant frequency that is relatively stable for the entire range.

3 PROOF OF PRINCIPLE

The tuning idea was first implemented by separating the cavity halves of a prototype with spacers that do not penetrate the cavity hollow volume or disturb the electromagnetic field pattern. The prototype was made of non-magnetic stainless steel (316 LN) coated with a 30 μm copper layer. The reason for choosing stainless steel as a base material for the cavity and not producing it from pure copper is the forces the cavity can be exposed to during a quench of the magnet (eddy currents). Cavities for axion Dark Matter searches are usually installed in multitesla fields.

A photograph of the prototype and spacers is shown in Fig. 7. The top picture shows the disassembled cavity halves and the spacers made of brass. These spacers generate a gap of around 1.25 mm and they are mounted on the screws that connect the two cavity halves. The bottom picture depicts the assembled cavity with spacers made of stainless steel. These spacers are commercially available washers mounted on the screws that keep the cavity halves together. The thickness of one washer is about 0.5 mm. Using several washers in a stack, gap sizes up to 2.5 mm were realised to characterise the cavity prototype at ambient conditions for different gap openings. After a characterisation of the tuning properties of the cavity at room temperature, the cavity was installed in a cryostat, and the unloaded quality factor Q_0 was measured between 7 and 300 K for a gap size of 0 and 1.25 mm. The brass spacers were used during the cryogenic characterisation. In none of the described mounting situations, the spacers entered the cavity structure. The alignment of the two halves of the cavity with each other depended only on the two spacers and the force with which the screws were tightened on each side. Both cavity ports were kept on one cavity half when a gap was applied.
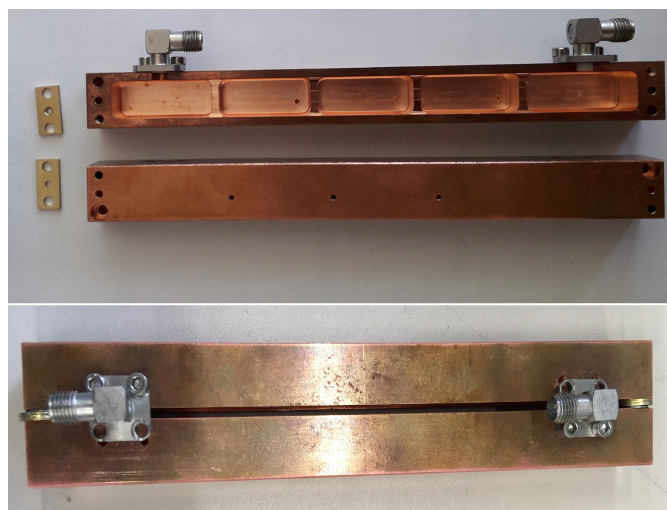

Figure 7. Photograph of the vertical cut haloscope coated with copper before assembly and brass spacers (top) and after assembly with a gap between the two halves introduced with stainless steel washer spacer (bottom). Note that for the characterisation both ports were attached to one cavity half unlike shown on the picture in which each port is attached to another cavity half.

Fig. 8 (left) shows measurements of the tuning range and quality factor at ambient conditions for a gap opening step size of 0.5 mm. A stack of stainless spacers was used to create the different gap sizes. There is a linear dependence between gap size and frequency, as expected, and the total tuning range at ambient conditions is 676 MHz for a gap opening of 2.5 mm. For bigger gap opening a decrease in quality factor up to 35 % for a 2.5 mm gap was observed during this test. From simulations in section 2.2.2 we know

that these losses can be attributed to misalignment. As not all spacers have exactly the same thickness, this uncertainty adds up when adding more spacers for a wider gap.
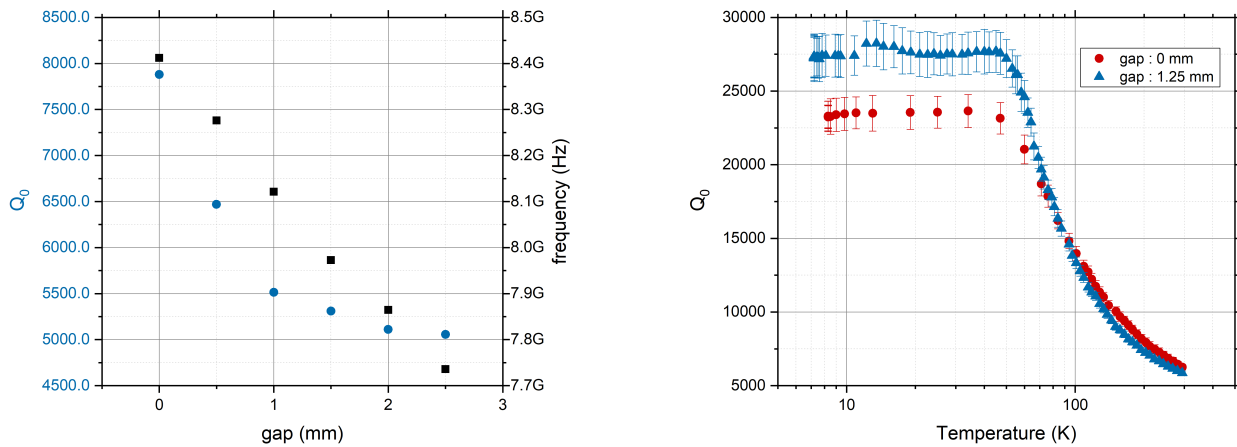

Figure 8. Unloaded quality factor Q_0 and resonant frequency for different gap sizes which were generated by spacers from washers (left) and Q_0 of the cavity between 7 and 300 K for gap sizes of 0 (red) and 1.25 mm (blue) using brass spacers (right).

For the characterisation at low temperature, the cavity was installed in a vacuum chamber which was introduced in a helium cryostat. The cavity was suspended in the cryostat by clamping it in a support structure on one extremity and subsequently attached to a long rod. It was measured in two configurations during cool-down for a gap size of 0 and 1.25 mm (half the maximum possible opening within the holding structure mechanics) separated by the brass spacers shown in Fig. 7 (top). The results from the cryogenic measurements of the quality factor with spacers are shown in Fig. 8 (right). For the cavity installed in the cryostat, the quality factors of Q_0 (gap = 0 mm) = 6300 ± 200 and Q_0 (gap = 1.25 mm) = 5950 ± 130 were measured at ambient conditions for the respective openings. The quality factor of the cavity installed in the cryostat and with no gap is lower than measured for the same cavity outside the cryostat (Q_0 = 7880 ± 20). These losses may be caused by some stresses applied to the cavity by the holding structure which can result in a misalignment of the cavity. Simulations showed that misalignments of 0.2 mm in $y-$axis direction can already cause a decrease in quality factor by more than 40 %, cf. section 2.2.2. During the cool-down, the cavity showed for both gap sizes the expected behaviour. The resonant frequency changed about 25 MHz between 300 and 40 K attributed to the thermal contraction of stainless steel. Below 40 K the resonant frequency is stable which is in good agreement with the behaviour of stainless steel regarding its thermal expansion at low temperatures.

Fig. 8 (right) shows that the quality factor for both configurations saturates around $40 - 50$ K. The copper coating of this cavity was applied by DC (Direct Current) galvanic plating with an organic brightener and the RRR (residual-resistance ratio) is expected to be 38 ± 2. The electrical conductivity for copper of this quality usually only saturates between 20 and 30 K, see Calatroni (2020b). The reason for these earlier saturations is the Anomalous Skin Effect (ASE). The cavity operates at frequencies above 8 GHz for the specified gap sizes. At those frequencies, the conductivity saturates once the mean free path of the electrons becomes bigger than the skin depth. Therefore, the electrical conductivity cannot increase further even if the mean free path increases. Changes below this temperature are attributed to other effects.

The unloaded quality factor at low temperatures was measured to Q_0 (gap= 0 mm, 8.3 K) = 23200 ± 800 and Q_0 (gap = 1.25 mm, 7.3 K) = 27200 ± 1500. For the cavity without a gap a higher quality factor was expected from simulations, see Fig. 4 (centre). But as mentioned previously the quality factor of the cavity after installation in the cryostat was already less than expected from measurements before the installation attributed probably to misalignment. The quality factor of the cavity with a gap was smaller at room temperature than for the configuration without a gap. During cool-down this ratio changed below 100 K. Due to the forces from the thermal contraction, the two cavity halves may have become better aligned and give values that are close to the values simulated, see Fig. 4 (centre), and in good agreement with the conductivity for copper considering ASE, see Calatroni (2020a).

4 TUNING MECHANISM FOR CRYOGENIC ENVIRONMENT

4.1 Set-up and sliding mechanism

After demonstrating that the tuning concept is viable in principle, a gear system was designed to allow for translating the movement in a cryogenic environment. For data-taking, haloscope axion cavities will be installed in dipole magnets where the space for tuning is typically limited by small bore diameters. Furthermore, the measurement takes place in a vacuum or liquid helium environment at temperatures of 4.2 K. These conditions make it challenging to realise cavity tuning during data-taking. Therefore, two
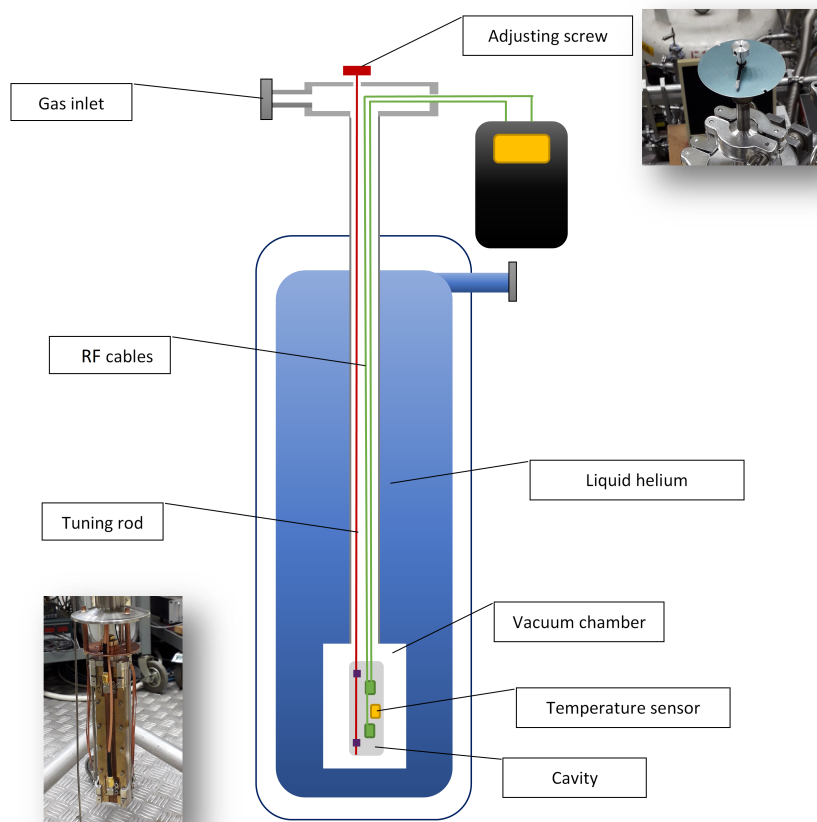

Figure 9. Cavity tuning test stand in the CERN Central Cryogenic laboratory with adjusting screw and rod (red), RF cables (green), temperature sensor (yellow), and the cavity (grey).
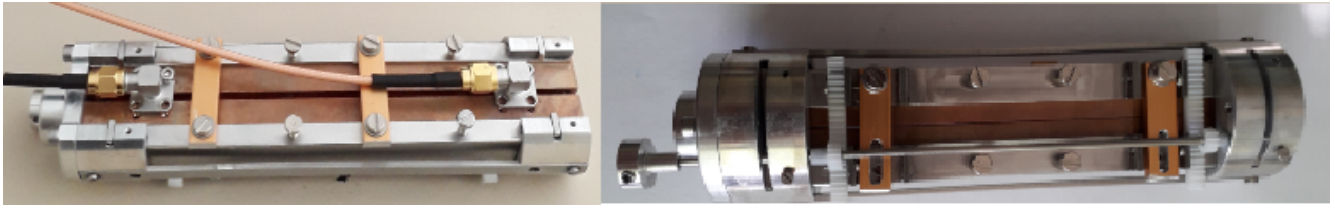
Figure 10. Photographs of the cavity halves installed in the tuning holding structure with gears. Top view with RF ports (left) and bottom view (right). The bottom view displays the gear mechanism that moves the cavity halves to each other.

possible solutions were deliberated. One option is to install a piezo actuator in the bore to generate the movement. However, two challenges have to be overcome: first, the space in the bore does not allow for a larger actuator. Secondly, an actuator with sufficient force to move the cavity halves is needed. Considering the size of the currently existing actuators that can move our cavity halves, a gear system to generate the movement would be necessary. Another possibility is to generate the movement from the outside of the magnet by a long rod connected via gears to the two cavity halves. This solution is also not without problems as complex feedthroughs are required to propagate the rotational movement from the 300 K to the 4 K environment.

To study the gear-based tuning mechanism, a test stand was built in the CERN Central Cryogenic Laboratory, and different aspects of this tuning were investigated. Fig. 9 shows a schematic drawing of the test stand. The cavity and the RF cables were installed in a vacuum chamber immersed in liquid helium. To characterise the cavity two RF cables (green) coming from the cavity were connected to a feedthrough in the vacuum flange at ambient temperature, to which a Vector Network Analyser (Keysight N9918A) was connected for quality factor measurements. To tune and change the gap size of the cavity a long rod (about 1.5 m long, 2 mm diameter, stainless steel) (red) was connected by a gear system to the cavity at the bottom of the vacuum chamber. The rod had an adjusting screw at the end and by turning it the cavity opened or closed, depending on the direction in which the gear is turned. The movement of the rod for this test was generated by hand, but the adjusting screw could be easily attached to a small motor which would allow more precision in movements. A gas inlet on the cryostat provided the possibility of measuring in a helium gas environment instead of in vacuum.

Photographs of the cavity installed in the holding system with gears to transmit the movement can be seen in Fig. 10. In Fig. 11, the individual parts of the tuning mechanism are shown. In (a), the holding pieces for the cavities are illustrated. The cavity halves can slide into these holding pieces, which are held by positioning screws. The holding piece has on both sides sliding bars. In Fig. 11 (b), the sliding structure is shown. The assembly consists of two of those structures that will be connected by long stainless steel bars, which have on one side long holes for easier positioning. The sliding bars shown in (a) have to be inserted in the sliding rails shown in (b). Fig. 11 (c) shows the assembly of (a) and (b) without cavities, and (d) shows the complete assembly with the cavity halves installed. The assembly shows the two gear racks that are screwed to holding piece (a) and a tuning rod with two gears glued to it. Thus, by turning this tuning rod outside of the cryostat, the rotation will be transmitted to the gears on the cavity inside the cryostat and converted into a linear, parallel translation of one cavity half.

To guarantee a smooth movement of the cavity halves with the described tuning mechanism at cryogenic temperatures and in vacuum, the materials have to be chosen carefully. In vacuum, parts of the same material can easily adhere to each other because there are no thin layers of other elements between the parts. Under mechanical pressure, e.g. thermal contraction, they can bond. Also, the friction coefficients between
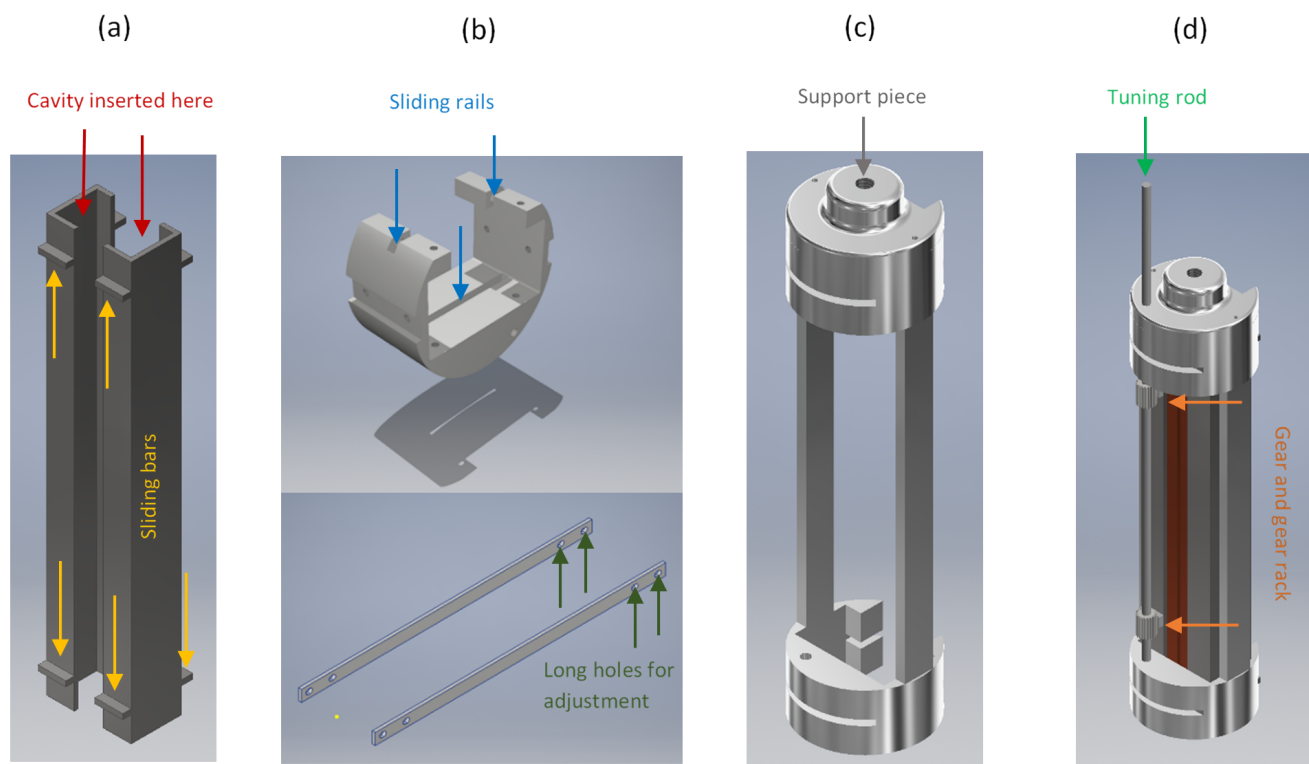
Figure 11. Drawings of the cavity support structure with (a) holding piece for the cavity halves, (b) the sliding structure for alignment, (c) the assembly of the sliding structure, and (d) the complete assembly with the gear system.

the same materials, i.e. aluminium on aluminium (friction coefficient $1.6 - 2.2$, c.f. Deulin et al. (2010)) or stainless steel on stainless steel (friction coefficient 2.9, see Deulin et al. (2010)), in vacuum are very high. Thus, it was decided to produce the holding pieces for the cavity and the holding structure out of different materials. The holding piece for the cavity was made of stainless steel (see Fig. 11 (a)) and the structure on which the cavity slides back and forth inside was made of aluminium (friction coefficient 0.3, see Deulin et al. (2010), and Fig. 11 (b)). The gear and gear rack were made of PTFE (Polytetrafluoroethylene) which has a very low friction coefficient of 0.04 for PTFE on PTFE, cf. Deulin et al. (2010).

After a first functionality test of the described mechanism and material, some optimisations have been made. The sliding structure (see Fig. 11 (a)) was re-fabricated using brass as it has a more similar expansion coefficient to aluminium than stainless steel. Furthermore, the holding pieces for the cavity were optimised by replacing the sliding bars with sliding pins, which have less surface area touching the sliding rail, resulting in reduced friction and less material deforming during cool-down.

4.2 Tuning results with the sliding mechanism

The tuning mechanism described in the previous section was tested on functionality at 77 K by immersing the set-up in liquid nitrogen. For testing a tuning mechanism where pieces are made of materials with different thermal expansion coefficients, it is crucial to wait for thermalisation. After a 5-minute thermalisation time in the liquid bath, an opening and closing of the cavity halves were demonstrated. The cavity spectrum and the tuning range were measured at ambient conditions, see Fig. 12 (left), and in liquid nitrogen, see Fig. 12 (right). The spectrum of the cavity shows five peaks, one for each of the small subcavities, while the axion only couples to the first mode. For explanations, see Álvarez Melcón et al.
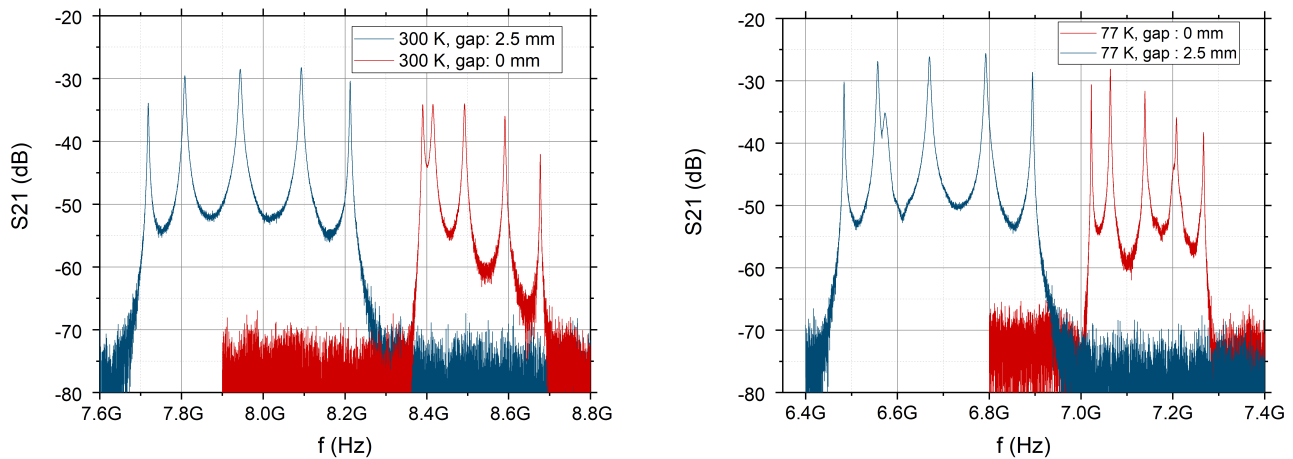
Figure 12. Tuning range measured with the cavity embedded in the sliding structure at ambient conditions (left) and in liquid nitrogen (right) with a maximum gap size of 2.5 mm (blue) and no gap (red). At 77 K disturbances of the spectra due to the boiling of liquid nitrogen are visible, most clearly for the second cavity peak in the spectra of the cavity with a 2.5 mm gap.

(2018). The difference in frequency between the first peak of each spectrum (and thus the tuning range) in the open (gap= 2.5 mm) and closed (gap= 0 mm) positions of the cavity halves was measured to be 670 MHz at ambient condition and 540 MHz in liquid nitrogen at 77 K. The tuning range in liquid nitrogen is smaller compared to air because the higher dielectric constant of LN_2 decreases the resonant frequency by a factor of $1/\sqrt{\varepsilon}$. The dielectric constant of liquid nitrogen is 1.431, see Mathes (1967), and therefore a tuning range of 540 MHz between 6.48 and 7.02 GHz corresponds to a tuning range in vacuum of about 650 MHz between 7.75 and 8.40 GHz.

In Fig. 12 (right) some disturbances in the second peak of the blue spectrum are visible. Those have their origin in gaseous Nitrogen bubbles that enter the cavity from time to time. Those bubbles are the result of the boiling of the liquid nitrogen and change the spectra while entering the cavity.

After demonstrating that the mechanism worked in a 77 K environment, the whole set-up was implemented in a cryostat with a 2 mm thick tuning rod of about 1.5 m length going from 4 to 300 K. The cavity and all elements were placed in a vacuum chamber inside the cryostat that was filled with liquid helium. A schematic of the experimental set-up is shown in Fig. 9. It was possible to reach temperatures around 20 K in the vacuum chamber with this setup. The reason for not reaching lower temperatures is the RF cables which are made of copper, a very good thermal conductor, as well as the tuning rod of 1.5 m length (stainless steel, 2 mm diameter) conducting heat from the outside of the cryostat at ambient temperature to the cold vacuum chamber. For measurements with spacers between the cavity halves, described in section 3, a minimum temperature of 6 K could be reached. However, this was only possible due to a complex thermalisation of the RF cables to intercept the conducted heat into the vacuum chamber. Those cables need to be moveable during tuning so as not to obstruct the mechanism, therefore they were not thermalised. Instead, thinner, more flexible cables were used with the disadvantage of higher RF losses.

The same results in terms of tuning are expected at 4 and 20 K, as previous measurements showed that the resonant frequency (= thermal contraction of the cavity) and quality factor (= electrical conductivity) for the cavity are constant below 30 K, see Fig. 8 (right). To use the cavity as a haloscope in an axion search, the temperature should be as low as possible. One possibility to solve the issue of not reaching the

minimum temperature is to let a small amount of exchange gas (about 1 mbar of helium) in the vacuum chamber, allowing convective heat transfer from the wall of the vacuum chamber to the cavity. By adding the exchange gas, the cavity properties remain the same, and the gas will not affect the haloscope data taking.
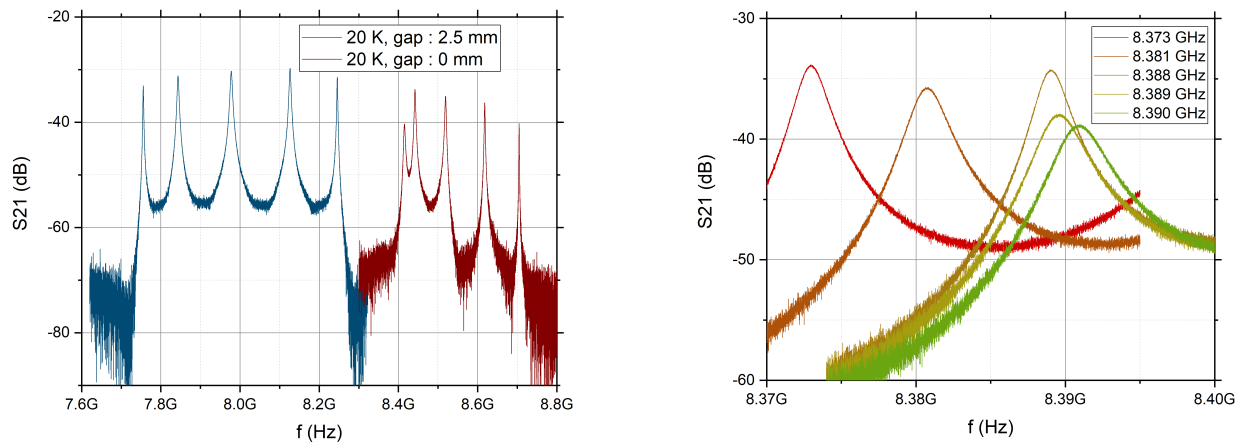

Figure 13. Tuning range measured with the cavity embedded in the sliding structure at 20 K with maximum gap size (blue) and without gap (red) (left). Zoom in on the first cavity peak (axion mode) for a selected set of cavity openings, demonstrating the minimum step size achieved for this measurement.

Fig. 13 shows the tuning results at 20 K. It was demonstrated that the cavity can be tuned in a cryogenic environment without performing a warm-up achieving a tuning range of 667 MHz. This result confirms the tuning range predicted from the measurement in liquid nitrogen described before. Besides the tuning range, a high scanning resolution is important to investigate all possible frequencies while a haloscope is data-taking. Therefore, frequency steps in the range of the 3 dB points of the resonant frequency should be realised. The frequency step size required to achieve this depends on the cavity properties: the unloaded quality factor (Q_0) and the coupling of the port. Assuming critical coupling and a Q_0 of 27000 (as measured for this specific cavity, see section 3) we aim for a step size of 0.6 MHz (8.4 GHz/13500) per step.

The described set-up reached a minimum step size of 3 MHz while the rotation was applied, turning an adjustment screw by hand; see Fig. 13 (right). Using a motor turning the adjustment screw at ambient conditions will lead to higher precision. Furthermore, high-precision gears and gear racks can help to decrease the frequency step size. To maximise the detection rate during tuning, over-coupling (i.e. $\beta = 2$) instead of critical coupling is more advantageous, cf.Kim et al. (2020). In that case, the minimum required step size required for our cavity increases to 0.9 MHz.

The cavity must maintain a high-quality factor during tuning. Therefore, Q_0 of the cavity was observed while changing the resonant frequency with the tuning mechanism and compared with the results obtained with the spacers, described in section 3. The result of the unloaded quality factor determination for different resonant frequencies of the cavity is illustrated in Fig. 14.

From the simulation in section 2.2.1 we expect a quality factor of about 27000 at cryogenic temperatures which does not degrade too much for a gap of 1.25 mm, cf. Fig. 4 (centre). Fig. 14 shows that this is hard to achieve. The blue points mark the measurements done with a spacer (gap= 1.25 mm) or the cavity bolted together with screws (gap = 0 mm). The measurements of those configurations were already partially
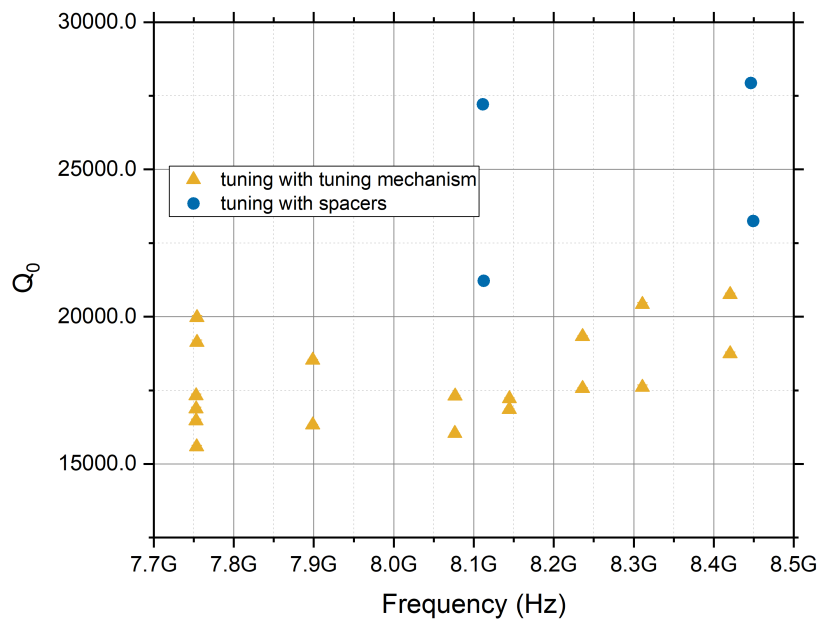
Figure 14. Unloaded quality factor (Q_0) of the cavity for different gap sizes generated by the tuning mechanism (yellow) and by spacers (blue) measured at cryogenic temperatures below 20 K.

discussed in section 3, where the quality factor for no gap turned out smaller than with a gap of 1.25 mm, most probably due to misalignment while installation. Both measurements were repeated, and different quality factors for the same gap size/resonant frequency were obtained, as shown in the graph. Only considering the maximum Q_0 measured for both spacer configurations (gap$= 0$ and 1.25 mm) the results are in good agreement with the simulations from section 2.2.1 for parallel cavities. The lower values for Q_0 for the same spacer configurations are attributed to misalignments. The simulations of section 2.2.2 showed how sensitive the cavity is to certain misalignment directions. The results underline the importance of a good alignment mechanism for the tuning, as a good-aligned setup is already hard to achieve with spacers.

The yellow triangles are the results obtained when changing the resonant frequency with the tuning mechanism described in section 4.1. The quality factor is for all measurements below the values obtained with spacers and varies for the same resonant frequency. The maximum decrease in quality factor measured with the tuning mechanism compared to its optimal values for no gap (Q_0 about 27000) is about 45 %. These losses are also attributed to misalignments of the two cavity halves, which leads to the conclusion that the alignment mechanism still needs to be improved and tolerances for the production of future assemblies need to be reduced.

5 CONCLUSION AND OUTLOOK

We have presented a concept to tune rectangular cavities for haloscope searches mechanically. The concept foresees cutting cavities along a symmetry plane of the field lines. We have validated this mechanism in practice and simulation. Assuming that the cavities are kept parallel, the simulations in section 2.2.1 predict a tuning range of up to 1.1 GHz (12.6 %) with nearly no degradation in the figure of merit ($Q_0 V^2 C^2$) over the whole range.

The cavity could be tuned in a range of 667 MHz ~ 9.5 % at 20 K using the sliding mechanism outlined in section 4.1. The available bore size limited the maximum gap size (2.5 mm) and hence the tuning range for the presented configuration. The obtained unloaded quality factor varied between $(1.5 - 2.1) \times 10^4$ while tuning. From the simulations in section 2.2.1 higher quality factors were expected. As can be observed from the simulations in section 2.2.2, the misalignment of the two cavity halves is the source of the losses (up to 45 %) in this assembly. Previous measurements in section 1 showed that greater values of Q_0 (2.7×10^4 at 7 K, gap= 1.25 mm) are possible for parallel cavity-halves (separated by spacers). This number is consistent with the parallel cavity-half simulations shown in section 2.2.1.

Moreover, misalignment can cause a 60 % decrease in form factor C; see Fig. 6. This is particularly relevant for cavity designs with subcavities connected by irises, as the misalignment alters the ideal operating mode conditions. Examining the same misalignment for a long single cavity, merely a minor deterioration of the form factor (0.66 to 0.63) is discernible.

The minimum step size achieved for this mechanism was 3 MHz. To have continuous tuning steps overlapping in their 3 dB range a step size of less than 0.9 MHz (3 μm) is required. To improve the step size of the assembly, high-precision gears and a motor-driven adjustment of the tuning rod are required.

The state of the art of various current tuning methods for different axion groups and the outcomes of this effort were displayed in Table 1 of section 1. The mechanical tuning presented in this work is a competitive way to tune an axion haloscope because it can achieve the same tuning percentage as the ADMX Sidecar - Run B while also having a larger form factor and quality factor. However, it is necessary to make improvements to the current tuning design to produce a smaller step size and handle the misalignment more effectively. Further studies using an improved gear mechanism, combined with a mechanism that moves the coupler are ongoing in the group.

APPENDIX

A. Misalignment due to coaxial ports

In this work, an additional misalignment study has been carried out on the haloscope with vertical cut tuning. The results obtained in section 2.2 are based on a system in which the coaxial ports are screwed to one of the two halves, causing a small misalignment or asymmetry in the total system. In this case, the behaviour of the structure has been analysed in simulation by positioning the coaxial ports centred in the middle of the opening of the structure (gap/2).

In Fig. 15 the results obtained in quality factor with a range of openings from gap= 0 to 2.5 mm are depicted. We can therefore conclude that this misalignment has practically no effect on this parameter and can be ignored in our system.

B. Misalignment in a long single cavity

In addition, the simulation of an individual cavity with the same dimensions of width, height and total length as the vertical cut multicavity (simply eliminating the inductive irises inside) has been carried out to observe the behaviour in form factor with angular misalignment in the $y-$axis (this is θ_y), which is the most relevant effect studied for this parameter (see Figure 6 (top-left corner plot)). The width of the single cavity is 22.86 mm, the width is 10.16 mm, and the length is 136.36 mm.

Applying a misalignment of $\theta_y = 0^o$ to 0.6^o, a range of detriment form factor values from 0.659 to 0.634 was obtained, confirming that the effect is not high for individual cavities. Thus, we can conclude that the
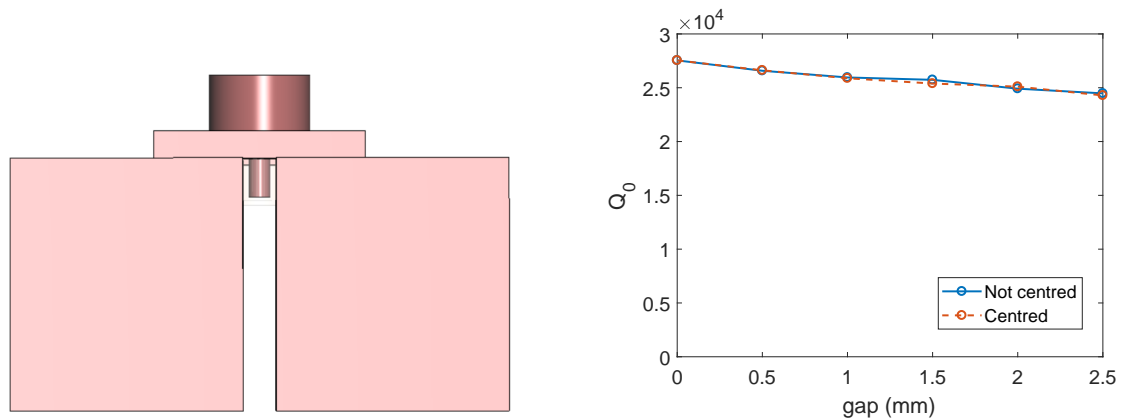
Figure 15. (Left) 3D model of the vertical cut structure with gap$= 2$ mm applying symmetry with the coaxial ports laying in the middle of the gap (centred at gap$/2 = 1$ mm), and (Right) quality factor results from CST simulations for this structure without (blue solid line) and with (red dashed line) centring the coaxial ports.

low form factor results obtained for the vertical cut haloscope with angular $y-$axis misalignment are due to the asynchrony of the individual frequencies of the subcavities of which it is composed.

6 KEYWORDS:

axion, haloscope, tuning, cryogenics, dark matter

CONFLICT OF INTEREST STATEMENT

The authors declare that the research was conducted in the absence of any commercial or financial relationships that could be construed as a potential conflict of interest.

AUTHOR CONTRIBUTIONS

JG carried out the measurements, performed data analyses, interpreted the results and contributed to the text. JMGB performed the cavity simulations and wrote the corresponding section. BD wrote parts of the text, acquired the funding to carry out the experiment, supervised the measurements, and contributed to interpreting the results. The initial idea of tuning with a vertical cut came from WW. He and SC also co-supervised the measurements and contributed to interpreting the results.

FUNDING

ACKNOWLEDGMENTS

DATA AVAILABILITY STATEMENT

Simulation data (3D model of the vertically cut cavity in ".stp" format) as well as plot data for the misalignment studies are available at the MPCDF MetaStore. Further data is available upon request.

REFERENCES

Adair, C. M. et al. (2022). Search for Dark Matter Axions with CAST-CAPP. *Nature Commun.* 13, 6180. doi:10.1038/s41467-022-33913-6

Ahyoune, S. et al. (2023). A proposal for a low-frequency axion search in the 1-2 μeV range and below with the BabyIAXO magnet doi:arXiv:2306.17243[physics.ins-det]

Aja, B., Cuendis, S. A., Arregui, I., Artal, E., Barreiro, R. B., Casas, F. J., et al. (2022). The canfranc axion detection experiment (cadex): search for axions at 90 ghz with kinetic inductance detectors. *Journal of Cosmology and Astroparticle Physics* 2022, 044. doi:10.1088/1475-7516/2022/11/044

Alesini, D., Braggio, C., Carugno, G., Crescini, N., D' Agostino, D., Di Gioacchino, D., et al. (2020). Realization of a high quality factor resonator with hollow dielectric cylinders for axion searches. *Nucl. Instrum. Methods. Phys. Res. B* 985, 164641. doi:10.1016/j.nima.2020.164641

Arguedas-Cuendis, S., Álvarez Melcón, A., Cogollos, C., Díaz-Morcillo, A., Döbrich, B., Gallego, J. D., et al. (2020). The 3 Cavity Prototypes of RADES: An Axion Detector Using Microwave Filters at CAST. In *Microwave Cavities and Detectors for Axion Research. Springer Proceedings in Physics*. vol. 245. doi:10.1007/978-3-030-43761-9_6

Bajjali, F. et al. (2023). First results from BRASS-p broadband searches for hidden photon dark matter. *JCAP* 08, 077. doi:10.1088/1475-7516/2023/08/077

Boutan, C., Jones, M., LaRoque, B. H., Oblath, N. S., Cervantes, R., Du, N., et al. (2018). Piezoelectrically Tuned Multimode Cavity Search for Axion Dark Matter. *Phys. Rev. Lett.* 121, 261302. doi:10.1103/PhysRevLett.121.261302

Braggio, C., Carugno, G., Di Vora, R., Ortolan, A., Ruoso, G., and Seyler, D. (2023). A tunable clamshell cavity for wavelike dark matter searches. *Review of Scientific Instruments* 94, 045111. doi:10.1063/5.0137621

Brun, P. et al. (2019). A new experimental approach to probe QCD axion dark matter in the mass range above 40 μeV. *Eur. Phys. J. C* 79, 186. doi:10.1140/epjc/s10052-019-6683-x

Calatroni, S. (2020a). A Mathematica Notebook for the calculation of the anomalous skin effect in copper doi:10.17181/CERN.MZIG.TJNX

Calatroni, S. (2020b). Materials & properties: Thermal & electrical characteristics

Choi, J., Ahn, S., Ko, B., Lee, S., and Semertzidis, Y. (2021). CAPP-8TB: Axion dark matter search experiment around 6.7 μev. *Nucl. Instrum. Methods. Phys. Res. B* 1013, 165667. doi:10.1016/j.nima.2021.165667

[Dataset] Computer Simulation Technology (CST) Studio Suite software (2023). `https://www.3ds.com/products-services/simulia/products/`

Deulin, E. A., Mikhailov, V. P., Panfilov, Y. V., and Nevshupa, R. A. (2010). *Friction in Vacuum* (Dordrecht: Springer Netherlands). 33–67. doi:10.1007/978-90-481-2520-3_3

Díaz-Morcillo, A., García Barceló, J. M., Lozano Guerrero, A. J., Navarro, P., Gimeno, B., Arguedas Cuendis, S., et al. (2022). Design of new resonant haloscopes in the search for the dark matter axion: A review of the first steps in the rades collaboration. *Universe* 8. doi:10.3390/universe8010005

García-Barceló, J. M., Díaz-Morcillo, A., and Gimeno, B. (2023). Enhancing resonant circular-section haloscopes for dark matter axion detection: approaches and limitations in volume expansion. *Journal of High Energy Physics* 2023, 159. doi:10.1007/JHEP11(2023)159

García Barceló, J. M., Álvarez Melcón, A., Arguedas Cuendis, S., Díaz-Morcillo, A., Gimeno, B., Kanareykin, A., et al. (2023). On the development of new tuning and inter-coupling techniques using ferroelectric materials in the detection of dark matter axions. *IEEE Access* 11, 30360–30372. doi:10.1109/ACCESS.2023.3260783

García-Barceló, J. M., Álvarez Melcón, A., Díaz-Morcillo, A., Gimeno, B., Lozano-Guerrero, A. J., Monzó-Cabrera, J., et al. (2023). Methods and restrictions to increase the volume of resonant rectangular-section haloscopes for detecting dark matter axions. *Journal of High Energy Physics* 2023, 98. doi:10.1007/JHEP08(2023)098

Gelmini, G. B., Millar, A. J., Takhistov, V., and Vitagliano, E. (2020). Probing dark photons with plasma haloscopes. *Phys. Rev. D* 102, 043003. doi:10.1103/PhysRevD.102.043003

Golm, J., Arguedas Cuendis, S., Calatroni, S., Cogollos, C., Döbrich, B., Gallego, J., et al. (2022). Thin film (high temperature) superconducting radiofrequency cavities for the search of axion dark matter. *IEEE Transactions on Applied Superconductivity* 32, 1–5. doi:10.1109/TASC.2022.3147741

Irastorza, I. G. and Redondo, J. (2018). New experimental approaches in the search for axion-like particles. *Prog. Part. Nucl. Phys.* 102, 89–159. doi:10.1016/j.ppnp.2018.05.003

Kim, D., Jeong, J., Youn, S., Kim, Y., and Semertzidis, Y. K. (2020). Revisiting the detection rate for axion haloscopes. *Journal of Cosmology and Astroparticle Physics* 2020, 066. doi:10.1088/1475-7516/2020/03/066

Knirck, S. et al. (2023). First Results from a Broadband Search for Dark Photon Dark Matter in the 44 to $52\,\mu$eV range with a coaxial dish antenna

Kuo, C.-L. (2021). Symmetrically tuned large-volume conic shell-cavities for axion searches. *Journal of Cosmology and Astroparticle Physics* 2021, 018. doi:10.1088/1475-7516/2021/02/018

Mathes, K. N. (1967). Dielectric properties of cryogenic liquids. *IEEE Transactions on Electrical Insulation* EI-2, 24–32. doi:10.1109/TEI.1967.298846

McAllister, B. T., Quiskamp, A. P., and Tobar, M. E. (2023). Tunable Rectangular Resonant Cavities for Axion Haloscopes

Miceli, L. (2015). Haloscope axion searches with the cast dipole magnet: the CAST-CAPP/IBS detector. In *11th Patras Workshop on Axions, WIMPs and WISPs*. 164–168. doi:10.3204/DESY-PROC-2015-02/miceli_lino

Peccei, R. and Quinn, H. (1977a). Constraints imposed by CP conservation in the presence of pseudoparticles. *Phys. Rev. D* 16, 1791–1797. doi:https://doi.org/10.1103/PhysRevD.16.1791

Peccei, R. and Quinn, H. (1977b). CP conservation in the presence of pseudoparticles. *Phys. Rev. Lett.* 38, 1440–1443. doi:https://doi.org/10.1103/PhysRevLett.38.1440

Pozar, D. M. (2012). *Microwave Engineering* (John Wiley and Sons, Inc.), fourth edn.

Primakoff, H. (1951). Photoproduction of neutral mesons in nuclear electric fields and the mean life of the neutral meson. *Phys. Rev.* 81, 899. doi:https://doi.org/10.1103/PhysRev.81.899

Rezaee, P., Knöchel, R., and Tayarani, M. (2012). Simple, fast, and accurate parametric modeling of the coupling and external quality factor for microstrip filter design using active learning method. *AEU - International Journal of Electronics and Communications* 66, 668–676. doi:https://doi.org/10.1016/j.aeue.2011.12.007

Sikivie, P. (1983). Experimental Tests of the Invisible Axion. *Phys. Rev. Lett.* 51, 1415–1417. doi:10.1103/PhysRevLett.51.1415. [Erratum: Phys.Rev.Lett. 52, 695 (1984)]

Zhong, L., Al Kenany, S., Backes, K. M., Brubaker, B. M., Cahn, S. B., Carosi, G., et al. (2018). Results from phase 1 of the HAYSTAC microwave cavity axion experiment. *Phys. Rev. D* 97, 092001. doi:10.1103/PhysRevD.97.092001

Álvarez Melcón, A., Arguedas-Cuendis, S., Baier, J., Barth, K., Bräuninger, H., Calatroni, S., et al. (2021). First results of the CAST-RADES haloscope search for axions at 34.67 microeV. *J. High Energ. Phys.* 2021, 75. doi:10.1007/JHEP10(2021)075

Álvarez Melcón, A., Arguedas-Cuendis, S., Cogollos, C., Díaz-Morcillo, A., Döbrich, B., Gallego, J. D., et al. (2018). Axion searches with microwave filters: the RADES project. *Journal of Cosmology and Astroparticle Physics* 040, 1–22. doi:10.1088/1475-7516/2018/05/040

Álvarez Melcón, A., Arguedas-Cuendis, S., Cogollos, C., Díaz-Morcillo, A., Döbrich, B., Gallego, J. D., et al. (2020). Scalable haloscopes for axion dark matter detection in the 30 μeV range with RADES. *Journal of High Energy Physics* 084, 1 – 28. doi:10.1007/JHEP07(2020)084